

Optical Spatial Modulation with Diversity Combiner in Dual-Hops Amplify-and-Forward Relay Systems Over Atmospheric Impairments

Kehinde Oluwasesan Odeyemi¹ · Pius Adewale Owolawi² ·
Viranjay M. Srivastava¹

Published online: 19 June 2017
© Springer Science+Business Media, LLC 2017

Abstract In this paper, we analyzed a dual-hop optical spatial modulation channel state information-assisted amplified and forward (AF) relay system with spatial diversity combiner under the influence of gamma-gamma atmospheric turbulence induced fading and pointing error impairments. Maximum ratio combiner (MRC) and equal gain combiner (EGC) with heterodyne detection are considered at the destination as mitigation tools to improve the system error performance. The statistical characteristics of AF relay in terms of moment generating function (MGF), probability density function and cumulative density function are derived for both impairments. Based on these expressions, the average pairwise error probability for each of the combiners under study is determined and the average bit error rate (ABER) for the system is given by using union bounding technique. By utilizing the derived ABER expressions, the effective capacity for the considered system is then obtained. The effect of turbulence strength ranging from weak to strong levels and pointing errors in terms of beam width and jitter displacement are studied. The numerical results obtained show that the more the turbulence strength and/or pointing error increases, the more the error rate and effective capacity of the system deteriorates. Under the same conditions, the results confirmed that MRC system offers an optimal performance compared with EGC.

Keywords Free space optical systems · Dual-hops transmission · Atmospheric turbulence · Spatial modulation · Diversity combiners · Amplified and forward relay

✉ Kehinde Oluwasesan Odeyemi
kesonics@yahoo.com

¹ Department of Electronic Engineering, Howard College, University of KwaZulu-Natal, Durban 4041, South Africa

² Department of Computer Systems Engineering, Tshwane University of Technology, Pretoria, South Africa

1 Introduction

Recently, there is tremendous increase in the need of high data and multimedia services such as high speed internet, video conferencing, live streaming which has led to the congestion in radio frequency (RF) spectrum. This has led to the need of changing from RF carrier to optical carrier [1]. Consequently, Free Space Optical (FSO) communication system has been proposed as alternative solution to this problem in recent times due to its various advantages. These include power consumption, cheap installation and operational cost, license-free spectrum, large bandwidth in the capacity of order of gigabytes, high level of security compare to RF systems counterpart [2, 3]. However, with these great attributes, the performance of FSO communication system highly suffers from many challenges. These challenges include atmospheric turbulence induced fading due to fluctuation in the refraction index as a result of inhomogeneous variation in temperature and pressure along the FSO link [4]. Hence, various statistical distributions have been proposed to model the atmospheric turbulence along the FSO link. One of such is lognormal distribution which is proposed for weak turbulence over a distance of less than 1 km [5]. Also, the K-distribution and negative exponential distribution have been studied to fit and offer accurate result for saturated turbulence strength over a long distance of several kilometers [6, 7]. Furthermore, Andrew et al. [8] proposed Gamma–Gamma distribution as the best distribution that agrees well with experimental data to model atmospheric turbulent from weak to strong levels. In addition to atmospheric turbulence, pointing error effect can also degrade the performance of FSO system as a result of building sway caused by dynamic wind loads, thermal expansion and weak earthquake. These cause vibrations in the transmitted beam leading to misalignment between the transmitter and receiver and limit the system performance [9]. Beside the building sway, as the link distance between the transmitter and receiver increases, the more the misalignment effect becomes pronounced, especially over a distance of 1 km or more [10]. The combined effect of these impairments on FSO link has been studied in literatures [11–13] and different techniques have been suggested to improve the system performance and availability over a long distance.

Studies have shown that the atmospheric turbulence induced fading and pointing error issues along the FSO link can be mitigated by using relay transmission technique [14]. This technique involves scaling down the distance between the transmitter and receiver through the use of relay hops in order to reduce the problem of a single transmitter to reach its intended target with necessary Signal to Noise Ratio (SNR). This concept was first explored by Acampora, and Krishnamurthy in [15], and few years later, the effectiveness of the relay system over a large coverage area was later studied in [16, 17]. The scheme has advantage of increasing the wireless systems coverage area to several kilometers without the needs of large power at the transmitter and relay units. It can also provide high data rate with low bit error at the end-to-end communication [18]. In this case, relay protocol can be classified into two and these include Decode-and-Forward (DF) relay that decodes any received signal from the source, re-encodes and then re-transmits the decoded information to the destination. This relay system is called regenerative relay system. The other type is Amplified-and-Forward (AF) relay which amplifies any incoming signal from the source and retransmits it to the destination without performing any sort of decoding and this is called non-regenerative relay system [19, 20].

Dual-hop relay transmission with AF protocol has been recently proposed for FSO links. For instance, in [21], On/Off Key (OOK) modulation was used to study the capacity performance of FSO dual-hops AF relay system with direct detection at the receiving end.

However, OOK modulation scheme requires selecting adaptive thresholds appropriately in order to achieve optimal performance, but it also suffers from poor power efficiency [22]. Moreover, Aggarwal et al. [23] investigate the performance of Subcarrier Intensity Modulation (SIM) dual-hops CSI-assisted AF relay with direct detection over turbulence channel with pointing error. However, the SIM modulation technique employed in this study offers a significantly higher transceiver complexity as the number of subcarrier increases. It also causes poor optical average power efficiency due to the increase in the number of required DC biases [24]. Moreover, a coherent FSO AF relaying system was considered by Pack et al. [25] in which the outage probability performance of the system was studied. Nevertheless, the proposed system is a single input single output (SISO) which is usually prone to pointing errors.

The concept of Spatial Modulation (SM) has been proposed as migration technique in FSO communication systems as it was found useful in [26–28] to improve the system error performance. Thus, based on our study, it shows that this type of modulation scheme has been investigated with relay technology mostly in RF wireless systems [29–32] but has not been taken into consideration in FSO systems. SM has been known to be an efficient low complex Multiple Input Multiple Output (MIMO) technique compared with other conventional MIMO schemes. At a specific instance, it allows transmission of signal from the activated antenna while other antennas remain idle [33]. This scheme has advantages of avoiding inter-channel interference, eliminating the needs of inter-antenna synchronization, and provides a robust system against channel estimation errors [34, 35]. Moreover, in many FSO research studies, Spatial Diversity (SD) combiner has been extensively considered to combat turbulence fading and pointing errors in order to improve the signal strength over a long distance [36]. The most common employed combiner includes maximum ratio combiner (MRC), equal gain combiner (EGC) and selection combiner (SC) [37]. Arguably, the combination of SM with diversity combiner as a powerful mitigation tool against fading impairments has not been investigated in FSO relaying systems. Motivated by this fact, we present the analysis of average BER and effective capacity of a dual-hop spatial modulation CSI-assisted AF relay system with diversity combiner over atmospheric turbulence and/or pointing error. In this case, the close form expression for the end-to-end SNR MGF, PDF and CDF are derived. Utilizing these results, the APEP for each combiner is determined and generic close form expression for the proposed system ABER is then obtained using union bounding technique. In consequence, the effective capacity for the system is determined through the derived ABER.

The rest of this paper is organized as follows: Sect. 2 presents the system model and the channel statistical model is discussed in Sect. 3. In Sect. 4, the statistical characteristics of end-to-end SNR are presented, while Sect. 5 presents the performance analysis of the system. Numerical and simulation results for the system performance, with their interpretation are presented in Sect. 6. Finally, the concluding remarks are outlined in Sect. 7.

2 System Model

Figure 1 illustrates a dual-hop SM-based relay FSO system with the source (S) as transmitter, destination (D) as receiver and Relay (R). We assume that the S-to-R and R-to-D links are independent, non-identical channel and heterodyne detection is used at R and D. The Source and the Destination are respectively equipped with N_t^S transmit lasers and N_r^D photo-detectors. The relay (R) in the system operates as Channel State Information (CSI)-

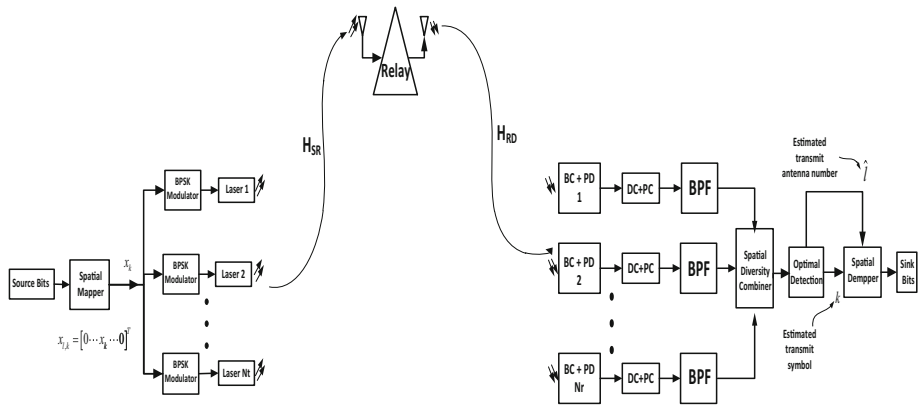


Fig. 1 Dual-hops SM-SD amplify-and-forward relay FSO system where *PD* photo-detector, *BC* beam combiner, *DC* down converter, *PC* phase compensator, *BPF* bandpass filter

assisted AF protocol and the destination employed spatial diversity combiner such as MRC and EGC. The system conducts transmission in two time slots. In the first phase, at the source, random sequence of bits stream to be transmitted are mapped into block of q -bits that is $q = \log_2(N_t M)$ of $X = [x_1, x_2, x_3 \dots x_{N_t}]^T$. The first group of these bits $\log_2(N_t)$ are used to represent the transmit laser index j th with the laser array while the remaining $\log_2(M)$ bits identify the BPSK modulation symbol x_p in the signal constellation. During this phase, the information bits are modulated on the electric field of an optical beam as $x_p = x_p \exp(j\phi_{x_p})$ and are then emitted from the active transmit-laser index j at an instance over the optical atmospheric channel as:

$$X_{jp} = \begin{bmatrix} 00 \dots 00 \dots \overbrace{x_p e^{j\phi_{x_p}}}^{j^{\text{th}} \text{ laser position}} \dots 00 \end{bmatrix}^T \tag{1}$$

At any instance of time, the received electric field at the aperture plane of the relay is sum of the optical field from the transmitter and the Local oscillator at the relay which can be expressed as [28, 38]:

$$E_R(t) = \sqrt{2P_t Z_o} |X_{jp} H_{SR}| \cos(\omega_{O,S} t + \phi_{h,S} + \phi_{x_p}) + \sqrt{2P_{LO} Z_o} \cos(\omega_{LO,R} t) \tag{2}$$

where $E_s(t) = \sqrt{2P_{t,S} Z_o} |X_{jp} H_{SR}| \cos(\omega_{O,S} t + \phi_{h,S} + \phi_{x_p})$ and $E_L(t) = \sqrt{2P_{LO,R} Z_o} \cos(\omega_{LO,R} t)$ are respectively the optical field from the transmitter and the LO field with Z_o denotes the free space impedance. $P_{t,S}$ is the transmit laser power from the source, while $P_{LO,R}$ is the relay LO power, and ω_{IF} is the intermediate frequency given as $\omega_{IF} = \omega_o - \omega_{LO,R}$ where $\omega_{o,S}$ and $\omega_{LO,R}$ denote the carrier frequency and relay LO frequency respectively. $H_{SR} = |h_{SR}| e^{j\phi_{h,S}}$ denotes the fading factor where the h_{SR} and $\phi_{h,S}$ are the fading gain and the link phase between the source and the relay.

The photocurrent at the relay photo-detector output can be obtained as [39]:

$$i_R(t) = \frac{R}{Z_o} [E_S(t) + E_L(t)]^2 \tag{3}$$

where $R = \eta q_e / (h\nu_o)$ is the responsivity of the photo-detector with electron charge $q_e = 1.6 \times 10^{-19} C$, and plank constant $h = 6.6 \times 10^{-34} Js$, η denotes the photo-detector efficiency and the optical central frequency $\nu_o = \omega_o / 2\pi$.

$$i_R(t) = RP_{t,S} |X_{jp} H_{SR}|^2 + RP_L + 2R \sqrt{P_t P_{LO,R}} |X_{jp} H_{SR}| \cos(\omega_{IF,R}t - \phi_{h,S} - \phi_{x_p}) \tag{4}$$

where $I_{DC,S} \triangleq RP_{t,S} |X_{jp} H_{SR}|^2$ and $I_{DC,L} \triangleq RP_{L,R}$ is the DC current generated due to signal and LO electric field respectively. $I_{AC} \triangleq 2R \sqrt{P_{t,S} P_{L,R}} |X_{jp} H_{SR}| \cos(\omega_{IF,R}t - \phi_{h,S} - \phi_{x_p})$ is the AC current which contains the useful information about the frequency and the phase of the received signal at the relay. The total output DC current at the photo-detector can be approximately equal to $RP_{L,R}$ [40]. Therefore, the short noise impaired during photo-detection process at this stage is dominated by LO short noise with variance of $\sigma_{short,L,R}^2 = 2q_e RP_{L,R} B_e$, where B_e is the electrical bandwidth of the photo-detector. In other words, the instantaneous signal-to-noise ratio (SNR) of the optical receiver can be defined as the time-average AC photocurrent and the total noise [40]. The SNR for the heterodyne relay receiver can be expressed as:

$$SNR_{(Het),SR} = \frac{\langle i_{AC}^2(t) \rangle}{2q_e RP_{L,R} B_e} \triangleq \frac{RP_t |X_{jp} H_{SR}|^2}{q_e B_e} \tag{5}$$

Based on the $SNR_{(Het),SR}$, the sufficient statistics at the relay can be modeled as [28, 38]:

$$y_R(t) = \sqrt{\bar{\gamma}_{SR}} H_{SR} X_{jp} + w_R(t) \tag{6}$$

where $\bar{\gamma}_{SR} = RP_t / (q_e \Delta f)$ is the average received SNR at the relay system and $w_R(t)$ is the noise term at the relay dominated by LO short noise model as Additive White Gaussian Noise (AWGN) with zero-mean and $\sigma_{short,L,R}^2$.

During the second phase, the photocurrent $i_R(t)$ at the relay photo-detector output is then amplified by the relay gain G , converted to optical signal and retransmitted to the destination. At the destination, using the same approach at the relay, the received optical signal at the n th heterodyne receiver at the destination can be expressed as:

$$E_{D,n}(t) = \sqrt{2P_{t,R} Z_o} |y_R(t) G H_{RD}| \cos(\omega_{O,R}t + \phi_{h,R}) + \sqrt{2P_{L,D}} \cos(\omega_{LO,D}t) \tag{7}$$

where $E_S(t) \triangleq \sqrt{2P_{t,R} Z_o} |y_R(t) G H_{RD}| \cos(\omega_{LO}t + \phi_{h,R})$ and $E_{L,D}(t) \triangleq \sqrt{2P_{L,D} Z_o} \cos(\omega_{LO,D}t)$ are the signal electric field transmitted by relay and LO electric field at the destination respectively. $H_{RD} \triangleq |h_{RD}| e^{j\phi_{h,R}}$ is the fading factor while the h_{RD} and $\phi_{h,R}$ are the fading gain and the link phase between the relay and the destination.

The photocurrent at the n th photo-detector at the destination can be similarly obtained as:

$$\begin{aligned}
 i_{D,n}(t) &= \frac{R}{Z_o} [E_s(t) + E_L(t)]^2 \\
 &\triangleq RP_{i,R}|y_R(t)GH_{RD}|^2 + RP_{L,R}GH_{RD} + 2R\sqrt{P_{i,R}P_{L,R}}|y_R(t)GH_{RD}|\cos(\omega_{IF}t - \phi_{h,R})
 \end{aligned}
 \tag{8}$$

where $I_{DC,s} \triangleq RP_{i,R}|y_R(t)GH_{RD}|^2$ and $I_{DC,L} \triangleq RP_{L,R}GH_{RD}$ is the DC current generated due to signal and LO electric field respectively at the n th heterodyne receiver at the destination while $I_{AC,D} \triangleq 2R\sqrt{P_{i,R}P_{L,R}}|y_R(t)GH_{RD}|\cos(\omega_{IF}t - \phi_{h,R})$ is the AC current which contains the useful information about the frequency and the phase of the received signal at the destination. The short noise impaired during photo-detection process at this stage is also dominated by destination LO short noise with variance of $\sigma_{short,L,D}^2 = 2q_eRP_{L,D}B_e$. The SNR on the R-to-D link for the n th heterodyne receiver can therefore be expressed as:

$$SNR_{(Het),RD} = \frac{\langle i_{AC,n}^2(t) \rangle}{2q_eRP_{L,D}B_e} \triangleq \frac{RP_{i,R}|y_R(t)GH_{RD}|^2}{q_eB_e}
 \tag{9}$$

The received signal at the n th heterodyne receiver can be statistically obtained as:

$$\begin{aligned}
 y_D(t) &= \sqrt{\gamma_{RD}}GH_{RD}y_R(t) + w_D(t) \triangleq \sqrt{\gamma_{RD}}GH_{RD} \left(\underbrace{\sqrt{\gamma_{SR}}H_{SR}X_{jp} + w_R(t)}_{\text{signal part}} \right) + w_D(t) \\
 &\triangleq \underbrace{\sqrt{\gamma_{RD}\gamma_{SR}}GH_{RD}H_{SR}X_{jp}}_{\text{signal part}} + \underbrace{\sqrt{\gamma_{RD}}GH_{RD}w_R(t) + w_D(t)}_{\text{Noise part}}
 \end{aligned}
 \tag{10}$$

In this paper, we assume that the receiver has full CSI and therefore after the normalization of the noise, the received signal at the n th heterodyne receiver at the destination can be further simplified as:

$$y_D(t) = \sqrt{K}H_{RD}X_{jp} + \hat{w}(t)
 \tag{11}$$

where $K = \frac{G^2H_{RD}^2\gamma_{RD}\gamma_{SR}}{\gamma_{RD}G^2H_{RD}^2+1}$ with G denoting the amplification factor at the relay and $\hat{w}(t)$ is the complex additive with Gaussian noise (AWGN) at the input of the destination having similar statistical characteristic as $w_R(t)$.

At destination, we assume optimum detection (OD) to detect the transmitted SM signal vector X_{jp} from the Source after the signal is combined by spatial diversity combiner. When the OD is applied, the estimated laser index \hat{J} and the transmitted constellation symbol index \hat{p} at a specific time instance can be expressed as [41]:

$$\begin{aligned}
 [\hat{J}, \hat{p}] &= \underset{\hat{J}, \hat{p}}{\operatorname{argmax}} p_Y(y_D | X_{jp}, H_{RD}) \\
 &\triangleq \underset{\hat{J}, \hat{p}}{\operatorname{argmin}} \sqrt{K} \|h_i^D x_p\|_F^2 - 2\operatorname{Re}\{y_D^H h_{RD} x_p\}
 \end{aligned}
 \tag{12}$$

The equivalent end-to-end SNR, which is the instantaneous received SNR at the destination, can be obtained as [19, 23, 42]:

$$\gamma_{eq} = \frac{\gamma_1\gamma_2}{\gamma_1 + \gamma_2} \triangleq \left(\sum_{i=1}^2 \frac{1}{\gamma_i} \right)^{-1}, i \in (1, 2)
 \tag{13}$$

where γ_1 and γ_2 are the instantaneous SNR at S-to-R and R-to-S links respectively which are defined in Eqs. (5) and (9). It is assumed that both link has equal average SNR obtained as $\bar{\gamma}_1 = \bar{\gamma}_2 = RP_t/(q_e\Delta f)$. Thus, the upper bound for the end-to-end SNR γ_{eq} can be derived by using the well-known inequality between geometric and harmonic means for the random variable $\bar{\gamma}_1$ and $\bar{\gamma}_2$ which is given as [19, 23]:

$$\gamma_{eq} \leq \gamma_a = \frac{1}{2} \prod_{i=1}^2 \gamma_i \tag{14}$$

3 Channel Statistical Model

The Gamma–Gamma was proposed by Andrew et al. for modeling FSO link with the conditions from weak to strong turbulence. This model probability distribution function (PDF) can be expressed as [43]:

$$f_{H_{mk}}(h) = \frac{2(\alpha\beta)^{\frac{\alpha+\beta}{2}}}{\Gamma(\alpha)\Gamma(\beta)} h^{\frac{\alpha+\beta}{2}-1} K_{\alpha-\beta}(2\sqrt{\alpha\beta h}), \quad h > 0 \tag{15}$$

where $\Gamma(\cdot)$ and $K_{(\cdot)}$ are defined as gamma function and v th order modified Bessel function of the 2nd kind respectively, α and β are the scintillation parameters which are specified as [44]:

$$\alpha = \left[\exp\left(\frac{0.49\sigma_R^2}{(1 + 1.11\sigma_R^{12/5})^{5/6}}\right) - 1 \right]^{-1}$$

$$\beta = \left[\exp\left(\frac{0.51\sigma_R^2}{(1 + 0.69\sigma_R^{12/5})^{5/6}}\right) - 1 \right]^{-1} \tag{16}$$

where $\sigma_R^2 = 0.49C_n^2(2\pi/\lambda)^{7/6}L^{11/6}$ is the Rytov Variation which is assumed to be spherical wave with λ stated as the optical wavelength, while L is the link range and C_n^2 is the refractive structure parameter that defines the turbulence strength [44].

Expressing $K_v(x)$ in terms of Meijer-G function [45], Eq. (14):

$$K_v(x) = \frac{1}{2} G_{0,2}^{2,0} \left(\frac{x^2}{4} \middle| \begin{matrix} - \\ v, -v \end{matrix} \right) \tag{17}$$

So, we can express the PDF of the Gamma–Gamma channel define in (15) as:

$$f_{H_{mk}}(h) = \frac{(\alpha\beta)^{\frac{\alpha+\beta}{2}}}{\Gamma(\alpha)\Gamma(\beta)} h^{\frac{\alpha+\beta}{2}-1} G_{0,2}^{2,0} \left(\alpha\beta h \middle| \begin{matrix} - \\ \alpha - \beta, \beta - \alpha \end{matrix} \right), \quad h > 0 \tag{18}$$

Also, the Gamma–Gamma channel PDF can be defined in terms of generalized power series representation method of the modified Bessel function of the second kind as [44, 46]:

$$K_\nu(x) = \frac{\pi}{2 \sin(\pi\nu)} \sum_{l=0}^{\infty} \left[\frac{1}{\Gamma(l - \nu + 1)l!} \left(\frac{x}{2}\right)^{2l-\nu} - \frac{1}{\Gamma(l + \nu + 1)l!} \left(\frac{x}{2}\right)^{2l+\nu} \right] \tag{19}$$

where $\nu \notin \mathbb{Z}$ and $|x| < \infty$

Thus, the PDF in (5) can also be expressed as:

$$f_{H_{mk}}(h) = \sum_{l=0}^{\infty} [a_k(\alpha, \beta)h^{k+\beta-1} + a_k(\beta, \alpha)h^{k+\alpha-1}] \tag{20}$$

where

$$a_k(x, y) = \frac{\pi(xy)^{l+\beta}}{\sin(\pi(x - y))\Gamma(x)\Gamma(y)\Gamma(k - x + y)k!}$$

The misalignment fading due to pointing error (h_p) loss by considering the detector size, beam width, and jitter variance is modeled by Raleigh distribution given as [47, 48]:

$$f_{H_{mk}}(h_p) = \frac{\xi^2}{A_o^{\frac{\xi^2}{\sigma_s^2}}} h_p^{\frac{\xi^2}{\sigma_s^2} - 1}, 0 \leq h_p \leq A_o \tag{21}$$

where $\xi = w_e/2\sigma_s$ and w_e is the equivalent beam width at the receiving end, σ_s is the standard deviation of the pointing error displacement at the receiver, is given as $A_o = \text{erf}^2(\nu)$, $\nu = \sqrt{\pi/2}(r_a/w_L)$ where r_a denotes the radius of the receiver aperture and w_L is the beam waist radius at distance L. Considering the impact of pointing error impairment, the PDF of the combined channel can be expressed as [49]:

$$f_{H_{mk}}(h) = \frac{\alpha\beta\xi^2}{A_o\Gamma(\alpha)\Gamma(\beta)} G_{1,3}^{3,0} \left(\frac{\alpha\beta}{A_o} h \left| \xi^2 - 1, \alpha - 1, \beta - 1 \right. \right) \tag{22}$$

The PDF of γ_i is obtained by power transformation of (22) and is expressed as:

$$f_{\gamma_i}(\gamma_i) = \frac{\xi_i^2}{2\gamma_i\Gamma(\alpha_i)\Gamma(\beta_i)} G_{1,3}^{3,0} \left(\alpha_i\beta_i\sqrt{\frac{\gamma_i}{\gamma_i}} \left| \frac{\xi_i^2}{\xi_i^2} + 1 \right. \right) \tag{23}$$

4 Statistical Characteristics of End-to-End SNR

4.1 Under the Influence of Atmospheric Turbulence Without Pointing Error

In this section, we derive the MGF, PDF and CDF of the end-to-end SNR γ_a defined in (14), with the assumption that the channel is independent non-identical distribution Gamma–Gamma turbulence channel.

4.1.1 MGF of the End-to-End SNR γ_a

The MGF of the end-to-end SNR γ_a can be derived in closed form as:

$$\begin{aligned}
 M_{\gamma_a}(-S) &= \int_0^\infty \int_0^\infty \left[\exp - \left(S \prod_{i=1}^2 \gamma_i^{1/2} \right) \right] \left[\prod_{i=1}^2 f_{\gamma_i}(\gamma_i) \right] d\gamma_i \\
 &\triangleq \int_0^\infty \int_0^\infty \exp \left(-S \gamma_1^{\frac{1}{2}} \gamma_2^{\frac{1}{2}} \right) f_{\gamma_1}(\gamma_1) f_{\gamma_2}(\gamma_2) d\gamma_1 d\gamma_2
 \end{aligned}
 \tag{24}$$

It should be noted that we can use the Gamma–Gamma PDF define in (18) and (20) to evaluate the MGF defined in (24). However, the integrals of the equation will yield infinite result and will be untraceable if we apply (20) to compute these integrals. Therefore we cannot obtain the exact close form expression for the end-to-end SNR. As a result of this, we thus applied the defined PDF in (18) to determine the MGF as follows:

If the PDF in terms of end-to-end SNR for the Gamma–Gamma can be expressed as:

$$f_{\gamma_i}(\gamma_i) = \frac{(\alpha_i \beta_i)^{\frac{\alpha_i + \beta_i}{2}} \gamma_i^{\frac{\alpha_i + \beta_i}{4} - 1}}{2\Gamma(\alpha_i)\Gamma(\beta_i)\gamma_i^{\frac{\alpha_i + \beta_i}{4}}} G_{0,2}^{2,0} \left(\frac{\alpha\beta}{\sqrt{\gamma_i}} \sqrt{\gamma_i} \left| \frac{-, -}{2}, \frac{\alpha_i - \beta_i, \beta_i - \alpha_i}{2} \right. \right)
 \tag{25}$$

If we let the $\Xi_i = \frac{\alpha\beta}{\sqrt{\gamma_i}}$ and apply the Meijer-G identity defined in [50], Eq. (9.31.5)], then the PDF can be expressed as:

$$\begin{aligned}
 f_{\gamma_i}(\gamma_i) &= \frac{(\Xi_i \sqrt{\gamma_i})^{\frac{\alpha_i + \beta_i}{2}}}{2\Gamma(\alpha_i)\Gamma(\beta_i)} \gamma_i^{-1} G_{0,2}^{2,0} \left(\Xi_i \sqrt{\gamma_i} \left| \frac{-, -}{2}, \frac{\alpha_i - \beta_i, \beta_i - \alpha_i}{2} \right. \right) \\
 &\triangleq \frac{1}{2\Gamma(\alpha_i)\Gamma(\beta_i)} \gamma_i^{-1} G_{0,2}^{2,0} \left(\Xi_i \sqrt{\gamma_i} \left| \frac{-, -}{2}, \frac{\alpha_i, \beta_i}{2} \right. \right)
 \end{aligned}
 \tag{26}$$

The first integration in (24) on γ_1 is of the form:

$$\mathfrak{I}_1(S) = \frac{1}{2\Gamma(\alpha_1)\Gamma(\beta_1)} \int_0^\infty \gamma_1^{-1} G_{0,2}^{2,0} \left(\Xi_1 \sqrt{\gamma_1} \left| \frac{-, -}{2}, \frac{\alpha_1, \beta_1}{2} \right. \right) \exp(-SV\gamma_1^{1/2}) d\gamma_1
 \tag{27}$$

where $V = \frac{\sqrt{\gamma_2}}{2}$

Using the Meijer-G identity of the exponential function in [45], Eq. (11)] to (27), then,

$$\mathfrak{I}_1(S) = \frac{1}{2\Gamma(\alpha_1)\Gamma(\beta_1)} \int_0^\infty \gamma_1^{-1} G_{0,2}^{2,0} \left(\Xi_1 \sqrt{\gamma_1} \left| \frac{-, -}{2}, \frac{\alpha_1, \beta_1}{2} \right. \right) G_{0,1}^{1,0} (SV\gamma_1^{1/2} |_0) d\gamma_1
 \tag{28}$$

let $Z = \gamma_1^{1/2}$, $Z^2 = \gamma_1$, $\frac{d\gamma_1}{dZ} = 2Z$ and $d\gamma_1 = 2ZdZ$, then apply the Meijer-G identity in [45], Eq. (21)]

$$\mathfrak{I}_1(S) = \frac{1}{\Gamma(\alpha_1)\Gamma(\beta_1)} G_{2,1}^{1,2} \left(\frac{SV}{\Xi_1} \left| \begin{matrix} 1 - \alpha_1, 1 - \beta_1 \\ 0 \end{matrix} \right. \right)
 \tag{29}$$

Using the similar method, the integration on γ_2 can be obtained by substituting (29) for (24):

$$\begin{aligned} \mathfrak{I}_2(S) &= \frac{1}{\Gamma(\alpha_1)\Gamma(\beta_1)} \frac{1}{2\Gamma(\alpha_2)\Gamma(\beta_2)} \int_0^\infty \gamma_1^{-1} G_{0,2}^{2,0} \left(\Xi_2 \sqrt{\gamma_2} \left| \begin{matrix} -, - \\ \frac{\alpha_2}{2}, \frac{\beta_2}{2} \end{matrix} \right. \right) G_{2,1}^{1,2} \left(\frac{SV}{\Xi_1} \sqrt{\gamma_2} \left| \begin{matrix} 1 - \alpha_1, 1 - \beta_1 \\ 0 \end{matrix} \right. \right) d\gamma_1 \\ &\triangleq \frac{1}{\Gamma(\alpha_1)\Gamma(\beta_1)} \frac{1}{\Gamma(\alpha_2)\Gamma(\beta_2)} G_{4,1}^{1,4} \left(\frac{SV}{\Xi_1 \Xi_2} \left| \begin{matrix} 1 - \alpha_1, 1 - \beta_1, 1 - \alpha_2, 1 - \beta_2 \\ 0 \end{matrix} \right. \right) \end{aligned} \tag{30}$$

Thus, substitute (29) and (30) for (24), then the MGF can be obtained as:

$$M_{\gamma_b}(S) = \prod_{i=1}^2 \frac{1}{\Gamma(\alpha_i)\Gamma(\beta_i)} G_{4,1}^{1,4} \left(\frac{S}{2\Xi_1 \Xi_2} \left| \begin{matrix} 1 - \alpha_1, 1 - \beta_1, 1 - \alpha_2, 1 - \beta_2 \\ 0 \end{matrix} \right. \right) \tag{31}$$

4.1.2 PDF of End-to-End SNR γ_a

The PDF of γ_b can be determined by applying the inversed Laplace Transform \mathcal{L}^{-1} to the MGF in (31) and this can be expressed as $f_{\gamma_a}(\gamma) = \mathcal{L}^{-1}\{M_{\gamma_a}(S), \gamma\}$. Applying the identity [51], Eq. (3.40.1.1)] for the inverse Laplace transform of the Meijer-G function, we obtained the PDF of γ_b in closed form as:

$$f_{\gamma_a}(\gamma) = \gamma^{-1} \prod_{i=1}^2 \frac{1}{\Gamma(\alpha_i)\Gamma(\beta_i)} G_{4,1}^{1,4} \left(2\gamma \prod_{i=1}^2 \Xi_i \left| \begin{matrix} - \\ \alpha_1, \beta_1, \alpha_2, \beta_2 \end{matrix} \right. \right) \tag{32}$$

4.1.3 CDF of End-to-End SNR γ_a

The CDF of the γ_a can be defined as $F_{\gamma_a}(\gamma) = \int_0^\gamma f_{\gamma_a}(\gamma) d\gamma$. Applying the integral identity stated in [45], Eq. (26), the CDF can therefore be obtained as follows:

$$\begin{aligned} F_{\gamma_b}(\gamma) &= \prod_{i=1}^2 \frac{1}{\Gamma(\alpha_i)\Gamma(\beta_i)} \int_0^\gamma \gamma^{-1} \prod_{i=1}^2 \frac{1}{\Gamma(\alpha_i)\Gamma(\beta_i)} G_{4,1}^{1,4} \left(2\gamma \prod_{i=1}^2 \Xi_i \left| \begin{matrix} - \\ \alpha_1, \beta_1, \alpha_2, \beta_2 \end{matrix} \right. \right) \\ &\triangleq \prod_{i=1}^2 \frac{1}{\Gamma(\alpha_i)\Gamma(\beta_i)} G_{1,5}^{4,1} \left(2\gamma \prod_{i=1}^2 \Xi_i \left| \begin{matrix} 1 \\ \alpha_1, \beta_1, \alpha_2, \beta_2, 0 \end{matrix} \right. \right) \end{aligned} \tag{33}$$

4.2 Under the Influence of Atmospheric Turbulence and Pointing Error

4.2.1 MGF of End-to-End SNR γ_a for the Pointing Error

Following the same approach used in obtaining the MGG of end-to-end SNR without pointing error, the MGF of end-to-end SNR with pointing error can thus be obtained by using (24), and the first integral on γ_1 is expressed as:

$$\mathfrak{I}_1(S) = \int_0^\infty \gamma_1^{-1} G_{1,3}^{3,0} \left(\alpha_1 \beta_1 \sqrt{\frac{\gamma_1}{\gamma_1}} \left| \begin{matrix} \xi_1^2 + 1 \\ \xi_1^2, \alpha_1, \beta_1 \end{matrix} \right. \right) G_{0,1}^{1,0} \left(SV \gamma_1^{1/2} \left| \begin{matrix} - \\ 0 \end{matrix} \right. \right) d\gamma_1 \tag{34}$$

By expressing the exponential function in form of Meijer-G function [50], Eq. (8.2.2)] and the integration of $\mathfrak{Z}_1(S)$ can be solved using [45], Eq. (21)] as:

$$\mathfrak{Z}_1(S) = 2G_{2,3}^{3,1} \left(\frac{\alpha_1 \beta_1}{SV\sqrt{\gamma_1}} \middle| 1, \xi_1^2 + 1 \right) \quad (35)$$

To solve the second integral in (24), substitute for $\mathfrak{Z}_1(S)$ and apply the Meijer-G identity given in [50], Eq. (8.2.2)] and [45], Eq. (21)], then the MGF is therefore obtained as:

$$M_{\gamma_a}(S) = \prod_{i=1}^2 \left[\frac{\xi_i^2}{\Gamma(\alpha_i)\Gamma(\beta_i)} \right] G_{3,6}^{6,1} \left(\frac{2}{S} \prod_{i=1}^2 \Xi_i \middle| 1, \psi_3 \right) \quad (36)$$

where $\psi_1 = \alpha_1, \beta_1, \alpha_2, \beta_2, \psi_2 = \xi_1^2, \xi_2^2$ and $\psi_3 = \xi_1^2 + 1, \xi_2^2 + 1$

4.2.2 PDF of End-to-End SNR γ_a for the Pointing Error

To determine the PDF of the end-to-end SNR, $f_{\gamma_a}(\gamma)$, apply inverse Laplace transform to (36) using the identity given in [51], Eq. (30.40.1.1)] as:

$$f_{\gamma_a}(\gamma) = \gamma^{-1} \prod_{i=1}^2 \left[\frac{\xi_i^2}{\Gamma(\alpha_i)\Gamma(\beta_i)} \right] G_{3,6}^{6,1} \left(2\gamma \prod_{i=1}^2 \Xi_i \middle| \psi_3 \right) \quad (37)$$

4.2.3 CDF of End-to-End SNR γ_a for the Pointing Error

The CDF for the end-to-end SNR can be obtained as $F_{\gamma_a}(\gamma) = \int_0^\gamma f_{\gamma_a}(\gamma) d\gamma$. Applying the integral identity stated in [45], Eq. (26)], the CDF can therefore be obtained as follows:

$$\begin{aligned} F_{\gamma_a}(\gamma) &= \int_0^\gamma \gamma^{-1} \prod_{i=1}^2 \left[\frac{\xi_i^2}{\Gamma(\alpha_i)\Gamma(\beta_i)} \right] G_{2,6}^{6,0} \left(2\gamma \prod_{i=1}^2 \Xi_i \middle| \psi_3 \right) d\gamma \\ &\triangleq \prod_{i=1}^2 \left[\frac{\xi_i^2}{\Gamma(\alpha_i)\Gamma(\beta_i)} \right] G_{3,6}^{6,1} \left(2\gamma \prod_{i=1}^2 \Xi_i \middle| 1, \psi_3 \right) \end{aligned} \quad (38)$$

5 Performance Analysis

At the destination, the receiver combines transmit amplified SM signal from the relay through the use of MRC and EGC. Thus, to determine the ABER for the proposed SM-SD dual-hop AF relay system, a well-known boundary technique is adopted to evaluate the BER under the fading condition. The average BER can be bounded as given in [41] by:

$$ABER_{SM-SD} \leq \frac{(N_t M)^{-1}}{\log_2(N_t M)} \sum_{j=1}^{N_t} \sum_{p=1}^M \sum_{j=j+1}^{N_t} \sum_{\hat{p}=p+1}^M N(p, \hat{p}) APEP(x_{j,p} \rightarrow x_{j,\hat{p}}) \quad (39)$$

where $N(p, \hat{p})$ is the number of bit error when selecting p instead of \hat{p} as the transmit unit index, $APEP(x_{j,p} \rightarrow x_{j,\hat{p}})$ denotes the Average Pairwise Error Probability (APEP) of deciding on the constellation vector $x_{j,p}$ given that $x_{j,\hat{p}}$ is transmitted.

5.1 Average Pairwise Error Probability for MRC Combiner

The instantaneous SNR at the output of MRC is defined as [52]:

$$\gamma_t^{MRC} = \sum_{n=1}^{N_r^p} \gamma_{a_n} \tag{40}$$

where γ_{a_n} is the end-to-end SNR received at the n th heterodyne receiver. Thus, the PEP can be expressed as:

$$\begin{aligned} PEP_{MRC}(x_{j,p} \rightarrow x_{j,\hat{p}}) &= Q\left(\sqrt{2\gamma_t^{MRC}}\right) \\ &\triangleq Q\left(\sqrt{2\sum_{n=1}^{N_r^p} \gamma_{a_n}}\right) \end{aligned} \tag{41}$$

Thus, by averaging (41), the average PEP for the MRC can be obtained as:

$$APEP_{MRC}(x_{j,p} \rightarrow x_{j,\hat{p}}) = \int_0^\infty \left(\sqrt{2\sum_{n=1}^{N_r^p} \gamma_{a_n}}\right) f_{\gamma_a}(\gamma) d\gamma \tag{42}$$

Using the upper bound of Crag’s Q-function defined as $Q(x) \leq 1/2 \exp(-x^2/2)$ [53], then the average PEP can be expressed as:

$$\begin{aligned} APEP_{MRC}(x_{j,p} \rightarrow x_{j,\hat{p}}) &= \frac{1}{2} \int_0^\infty \exp\left(-\sum_{n=1}^{N_r^p} \gamma_{a_n}\right) f_{\gamma_a}(\gamma) d\gamma \\ &\triangleq \frac{1}{2} \prod_{n=1}^{N_r^p} M_{\gamma_{a_n}}(S) \end{aligned} \tag{43}$$

To determine the average PEP for the MRC-SM under the influence of atmospheric turbulence without pointing error, substitute (31) for (43) as:

$$APEP_{MRC}(x_{j,p} \rightarrow x_{j,\hat{p}}) = \frac{1}{2} \left[\prod_{i=1}^2 \frac{1}{\Gamma(\alpha_i)\Gamma(\beta_i)} G_{4,1}^{1,4} \left(\frac{1}{2\Xi_1\Xi_2} \middle| 1-\alpha_1, 1-\beta_1, 1-\alpha_2, 1-\beta_2 \right)_0 \right]^{N_r^p} \tag{44}$$

Similarly, the average PEP for the MRC-SM under the influence of atmospheric turbulence with pointing error, substitute (36) for (43) as:

$$APEP_{MRC}(x_{j,p} \rightarrow x_{j,\hat{p}}) = \frac{1}{2} \left[\prod_{i=1}^2 \left[\frac{\xi_i^2}{\Gamma(\alpha_i)\Gamma(\beta_i)} \right] G_{3,6}^{6,1} \left(2 \prod_{i=1}^2 \Xi_i \middle| \begin{matrix} 1, \psi_3 \\ \psi_1, \psi_2 \end{matrix} \right) \right]^{N_r^D} \tag{45}$$

Thus, the average BER for the MRC dual-hop relay system without and with pointing error can therefore be respectively obtained by substituting (44) and (45) for (39):

$$ABER_{MRC(\text{without pointing error})} \leq \frac{(N_t M)^{-1}}{2 \log_2(N_t M)} \sum_{j=1}^{N_t} \sum_{p=1}^M \sum_{j=j+1}^{N_t} \sum_{\hat{p}=p+1}^M N(p, \hat{p}) \left[\prod_{i=1}^2 \frac{1}{\Gamma(\alpha_i)\Gamma(\beta_i)} G_{4,1}^{1,4} \left(\frac{1}{2\Xi_1\Xi_2} \middle| \begin{matrix} 1 - \alpha_1, 1 - \beta_1, 1 - \alpha_2, 1 - \beta_2 \\ 0 \end{matrix} \right) \right]^{N_r^D} \tag{46}$$

$$ABER_{MRC(\text{with pointing error})} \leq \frac{(N_t M)^{-1}}{2 \log_2(N_t M)} \sum_{j=1}^{N_t} \sum_{p=1}^M \sum_{j=j+1}^{N_t} \sum_{\hat{p}=p+1}^M N(p, \hat{p}) \left[\prod_{i=1}^2 \left[\frac{\xi_i^2}{\Gamma(\alpha_i)\Gamma(\beta_i)} \right] G_{3,6}^{6,1} \left(2 \prod_{i=1}^2 \Xi_i \middle| \begin{matrix} 1, \psi_3 \\ \psi_1, \psi_2 \end{matrix} \right) \right]^{N_r^D} \tag{47}$$

5.2 Average Pairwise Error Probability for EGC Combiner

The instantaneous SNR at the output of MRC is defined as [52]:

$$\gamma_r^{EGC} = \frac{1}{N_r^D} \left(\sum_{n=1}^{N_r^D} \sqrt{\gamma_{a_n}} \right)^2 \tag{48}$$

The approach detailed in [54, 55], $\gamma_T = \left(\sum_{n=1}^{N_r^D} \sqrt{\gamma_{a_n}} \right)^2$ with $\bar{\gamma}_T = N_r^D \bar{\gamma}, \alpha_{\gamma_T} = N_r^D \alpha + \varepsilon_\gamma, \beta_{\gamma_T} = N_r^D \beta$, denoting the adjustment parameter in order to improve the accuracy of proposed approximation [55] is defined as:

$$\varepsilon_\gamma = \left(\frac{1}{N_r^D} - 1 \right) \frac{-0.127 - 0.95\alpha - 0.0058\beta}{1 + 0.00124\alpha + 0.98\beta} \tag{49}$$

The average PEP for the EGC can be expressed as:

$$APEP_{EGC}(x_{j,p} \rightarrow x_{j,\hat{p}}) = \int_0^\infty \left(\sqrt{2\gamma_r^{EGC}} \right) f_{\gamma_a}(\gamma) d\gamma \tag{50}$$

$$\triangleq - \int_0^\infty Q' \left(\sqrt{2\gamma_r^{EGC}} \right) F_{\gamma_a}(\gamma) d\gamma$$

where $Q/(\cdot)$ is the derivative of Q-function which is defined in [57] as $Q/(x) = \frac{1}{2\sqrt{\pi}} \exp(-x^2/2)$

$$APEP_{EGC}(x_{j,p} \rightarrow x_{j,\hat{p}}) = \frac{1}{2\sqrt{\pi}} \int_0^\infty \frac{1}{\sqrt{\gamma_T}} \exp\left(-\frac{\gamma_T}{N_r^D}\right) F_{\gamma_a}(\gamma_T) d\gamma_T \tag{51}$$

To determine the APER for the EGC dual-hop AF system under the influence of atmospheric turbulence without pointing error, substitute the CDF defined in (33) for (50)

$$APEP_{EGC}(x_{j,p} \rightarrow x_{j,\hat{p}}) \triangleq \frac{1}{2\sqrt{\pi}} \prod_{i=1}^2 \left[\frac{1}{\Gamma(\alpha_{\gamma T_i}) \Gamma(\beta_{\gamma T_i})} \right] \int_0^\infty \gamma_T^{-1/2} \exp\left(-\frac{\gamma_T}{N_r^D}\right) G_{4,1}^{1,4} \times \left(2\gamma_T \prod_{i=1}^2 \Xi_i \middle| \begin{matrix} 1 \\ \alpha_{\gamma T_1}, \beta_{\gamma T_1}, \alpha_{\gamma T_2}, \beta_{\gamma T_2}, 0 \end{matrix} \right) d\gamma_T \tag{52}$$

Applying the integral indent defined in [50], Eq. (7.813.1)], the APER for the EGC dual-hop AF system under the influence of atmospheric turbulence without pointing error can be expressed as:

$$APEP_{EGC}(x_{j,p} \rightarrow x_{j,\hat{p}}) \triangleq \frac{1}{2} \sqrt{\frac{N_r^D}{\pi}} \prod_{i=1}^2 \left[\frac{1}{\Gamma(\alpha_{\gamma T_i}) \Gamma(\beta_{\gamma T_i})} \right] G_{2,5}^{4,2} \left(2N_r^D \prod_{i=1}^2 \Xi_i \middle| \begin{matrix} 1 \\ \alpha_{\gamma T_1}, \beta_{\gamma T_1}, \alpha_{\gamma T_2}, \beta_{\gamma T_2}, 0 \end{matrix} \right) \tag{53}$$

Under the influence of pointing error, using (38) in (51), the average PEP can be expressed as:

$$APEP_{EGC}(x_{j,p} \rightarrow x_{j,\hat{p}}) = \frac{1}{2\sqrt{\pi}} \prod_{i=1}^2 \left[\frac{\xi_i^2}{\Gamma(\alpha_{\gamma T_i}) \Gamma(\beta_{\gamma T_i})} \right] \int_0^\infty \gamma_T^{-1/2} \exp\left(-\frac{\gamma_T}{N_r^D}\right) G_{3,6}^{6,1} \times \left(2\gamma_T \prod_{i=1}^2 \Xi_i \middle| \begin{matrix} 1, \psi_3 \\ \psi_1, \psi_2 \end{matrix} \right) d\gamma_T \tag{54}$$

Applying the integral indent defined in [50], Eq. (7.813.1)], the APER for the EGC dual-hop AF system under the influence of atmospheric turbulence without pointing error can be expressed as:

$$APEP_{EGC}(x_{j,p} \rightarrow x_{j,\hat{p}}) = \frac{1}{2} \sqrt{\frac{N_r^D}{\pi}} \prod_{i=1}^2 \left[\frac{\xi_i^2}{\Gamma(\alpha_{\gamma T_i}) \Gamma(\beta_{\gamma T_i})} \right] G_{4,6}^{6,2} \left(2N_r^D \prod_{i=1}^2 \Xi_i \middle| \begin{matrix} 1 \\ \psi_1, \psi_2 \end{matrix} \right) \tag{55}$$

Thus, the average BER for the MRC dual hop relay system can therefore be obtained by substituting (53) and (55) for (39):

$$ABER_{EGC}(\text{with pointing error}) \leq \frac{(N_r M)^{-1}}{2 \log_2(N_r M)} \sqrt{\frac{N_r^D}{\pi}} \prod_{i=1}^2 \left[\frac{\xi_i^2}{\Gamma(\alpha_{\gamma T_i}) \Gamma(\beta_{\gamma T_i})} \right] \sum_{j=1}^{N_r} \sum_{p=1}^M \sum_{j=j+1}^{N_r} \sum_{\hat{p}=p+1}^M N(p, \hat{p}) \times G_{2,5}^{4,2} \left(2N_r^D \prod_{i=1}^2 \Xi_i \middle| \begin{matrix} 1 \\ \alpha_{\gamma T_1}, \beta_{\gamma T_1}, \alpha_{\gamma T_2}, \beta_{\gamma T_2}, 0 \end{matrix} \right) \tag{56}$$

$$\begin{aligned}
 ABER_{EGC(\text{with pointing error})} \leq & \frac{(N_t M)^{-1}}{2 \log_2(N_t M)} \sqrt{\frac{N_r^D}{\pi}} \prod_{i=1}^2 \left[\frac{\xi_i^2}{\Gamma(\alpha_{\gamma T_i}) \Gamma(\beta_{\gamma T_i})} \right] \sum_{j=1}^{N_t} \sum_{p=1}^M \sum_{j=j+1}^{N_t} \sum_{\hat{p}=\hat{p}+1}^M N(p, \hat{p}) G_{4,6}^{6,2} \\
 & \times \left(2N_r^D \prod_{i=1}^2 \Xi_i \left| \frac{1}{2}, 1, \psi_3 \right. \right) \\
 & \left. \psi_1, \psi_2 \right)
 \end{aligned} \tag{57}$$

5.3 Effective Capacity for the Systems

The capacity of spatial modulation systems as stated in [56–59] cannot be determined in the same way it is done in MIMO communication systems. This is because, the number of transmit antenna represents the added information, and antenna index signifies the spatial constellation not as the information source as in other MIMO systems. Therefore, using the convectional approach stated in [59], the capacity for the dual-hop spatial modulation with combiner can be expressed as:

$$C_{SM} = \log_2(N_t^s M) [1 + P_e \log_2(P_e) + P_c \log_2(P_c)] \tag{58}$$

where, P_e is the overall probability of error defined in Eq. (39), and $P_c = 1 - P_e$ represents the probability of correct detection and $\log_2(N_t^s M)$ defines the total bits convey by the system.

6 Numerical Results and Discussions

In this section, using the derived expression of Eqs. (46), (47), (56), (57) and (58), we present the effect of atmospheric turbulence and pointing error on the average BER and the effective capacity performance of optical SM-SD dual-hops CSI-assisted relay. Generally, we assume that the link between the S-R and R-D are symmetric atmospheric turbulence channel with weak ($\alpha = 3.78, \beta = 3.74$), moderate ($\alpha = 2.50, \beta = 2.06$) and strong ($\alpha = 2.04, \beta = 1.10$).

Fig. 2 Performance of dual-hops AF SM-MRC-FSO system under different atmospheric turbulence without pointing error When the $N_r^D = 2$ and $N_r^D = 4$

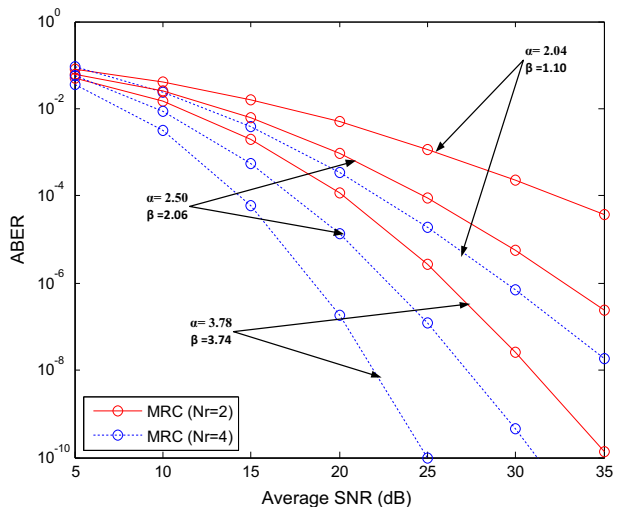


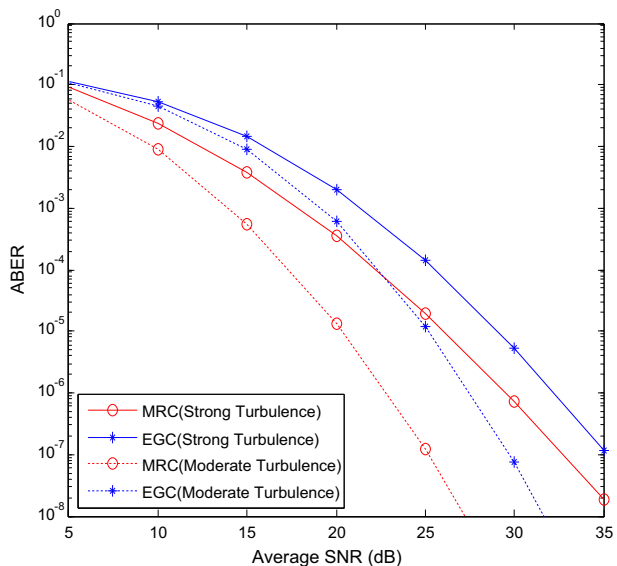
Figure 2 shows the effect of atmospheric turbulence conditions on the average BER on the system performance under different MIMO schemes when MRC is considered at the receiver. This result confirmed that the change in turbulence condition from weak to strong level significantly degrades the system performance. For instance, at average SNR of 25 dB when considering two PD at the receiver, it is discovered that atmospheric turbulence greatly degraded the system error by 99.76% between the weak and strong turbulence condition. However, this performance can be improved by increasing the number of PD. Thus, at average BER of 10^{-4} , it is shown that the MRC system with four PD offers a gain of 5 dB when compared with two PD system under the same weak turbulence.

The performance comparison between the MRC and EGC is presented in Fig. 3. It is clearly shown that the MRC yields an optimal performance than EGC under the same conditions. For instance, at average SNR of 20 dB under moderate turbulence condition, MRC offers an error rate of 1.32×10^{-5} compared with EGC of 6.20×10^{-4} .

We also illustrate the impact of beam width on the system error rate in Fig. 4. It is depicted in Fig. 4a that as the beam width increases the better the system error performance for the MRC system over a strong atmospheric turbulence for both MIMO schemes and is least with no pointing error. It can be deduced that with four PD, there is less error compared with two PD. For instance, when considering four PD at the MRC system, at average SNR of 20 dB, the system offers an error improvement of 97% by producing an error of 3.03×10^{-5} compared to 0.0015 average errors produced when using two PD. Moreover, the performance of the MRC dual-hops AF relay system is also compared with the EGC in Fig. 4b when using two PD at the receiving end. Under the strong turbulence condition, it is clearly shown that MRC offers a 2 dB diversity gain compared to EGC at the average BER of 10^{-2} .

The impact of pointing error on the dual-hop MRC AF relay system is demonstrated in Fig. 5a under different turbulence conditions. It clearly shows that as the pointing error increases from values 2 to 5, the more the system error rate deteriorates. For instance, under the strong turbulence condition, the pointing error value of 5 causes the MRC system

Fig. 3 Performance comparison between the EGC and MRC Dual-hop AF system under different atmospheric turbulence without pointing error when $N_r^D = 4$



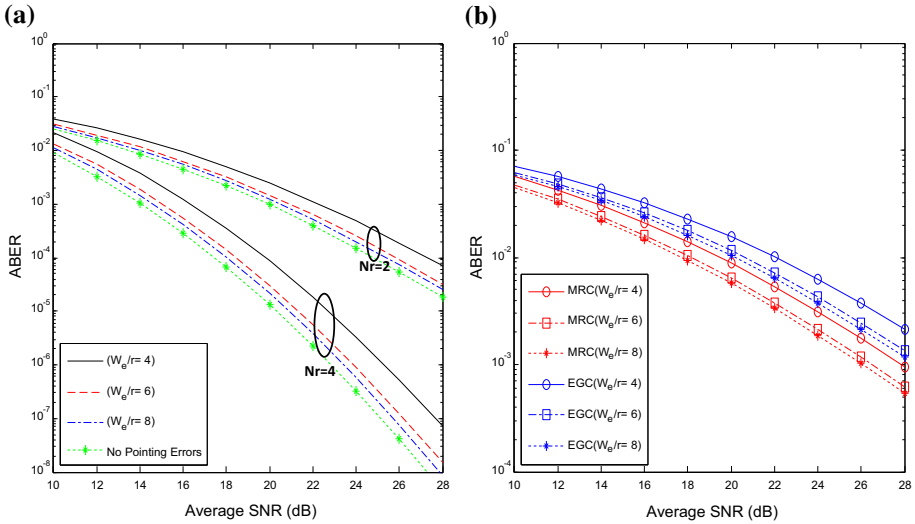


Fig. 4 **a** Impart of normalized beam width on the SM-MRC dual-hop AF system with different received photo-detector at the destination. **b** Performance comparison between the MRC and EGC dual-hop AF system under the influence of normalized beam width at $N_r^D = 2$

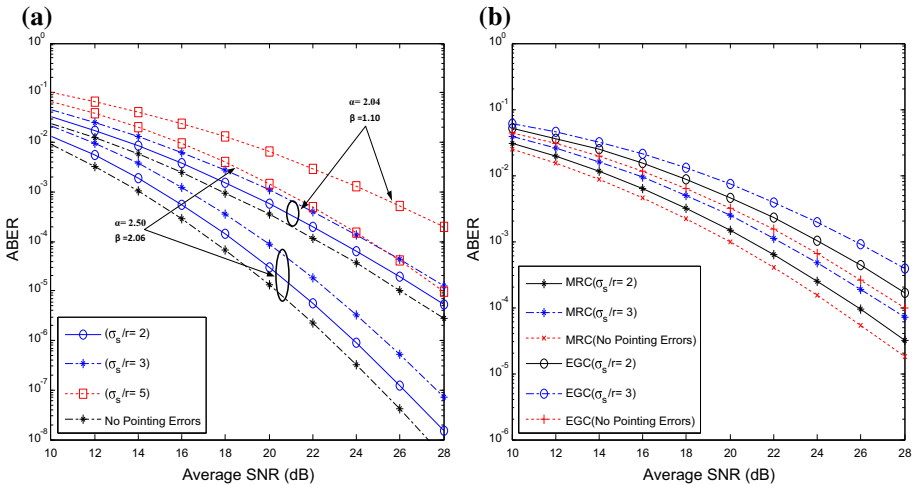


Fig. 5 **a** Impart of pointing error on the SM-MRC dual-hop AF system with different received photo-detector at the destination. **b** Performance comparison between the MRC and EGC dual-hop AF system under the influence of strong turbulence and pointing error at $N_r^D = 2$

to offer an average error of 0.0095 compared to when no pointing error is considered with error 2.25×10^{-4} . Under the same turbulence condition and pointing error, we compared the performance between the MRC with EGC in Fig. 5b. As expected, the MRC system offers the best performance compared to the EGC system for various values of pointing error. For instance, to achieve an average BER of 10^{-3} when pointing error value is set to

2, the MRC system requires only a power of 21 dB compare with EGC of 24 dB when the receiver is equipped with two PD.

In addition, the average error performance of the dual-hop MRC AF relay system is presented in Fig. 6a under different values of ζ and atmospheric turbulence ranging from weak to strong levels. It can be clearly depicted that the higher the value of ζ , the lower the system error rate and also the system performance deteriorates as the atmospheric turbulence condition gets worst. For instance, at average SNR of 20 dB under weak turbulence, there is a margin error of 3.93×10^{-4} between the two ζ values, and this shows that there is 74% error improvement when $\zeta = 6.5$ under the same average SNR. Comparing the MRC with EGC as it is demonstrated in Fig. 6a at a high value of $\zeta = 6.5$, it is found that at average BER of 10^{-3} , the MRC required a power of 20 dB compared to 25 dB for EGC.

The capacity performance of the dual-hop AF relay system is illustrated in Fig. 7 under different turbulence conditions without pointing error when considering both the MRC and EGC at the receiver. It is clearly confirmed that as the turbulence get sever, the more the capacity of the system deteriorates. It is also indicated in the result that the number of laser at the transmitter significantly improved the system capacity. For instance, at the average SNR of 14 dB, it is shown that MRC offers an effective capacity of 1.72 bit/s/Hz compared to 1.60 bits/s/Hz offered by EGC and the use of four lasers caused 32% increment in capacity for MRC under the same conditions.

Figure 8 illustrates the influence of both pointing error and turbulence on the MRC dual-hop AF system capacity. It is clearly shown that as the pointing error increases, the system capacity performance deteriorates for both when the laser is four and two at the transmitter as against when there is no pointing error. It is also confirmed that for a given turbulence condition and pointing error, the capacity of MRC with four lasers is higher compared to when the transmitter is equipped with two lasers. This proved that the higher

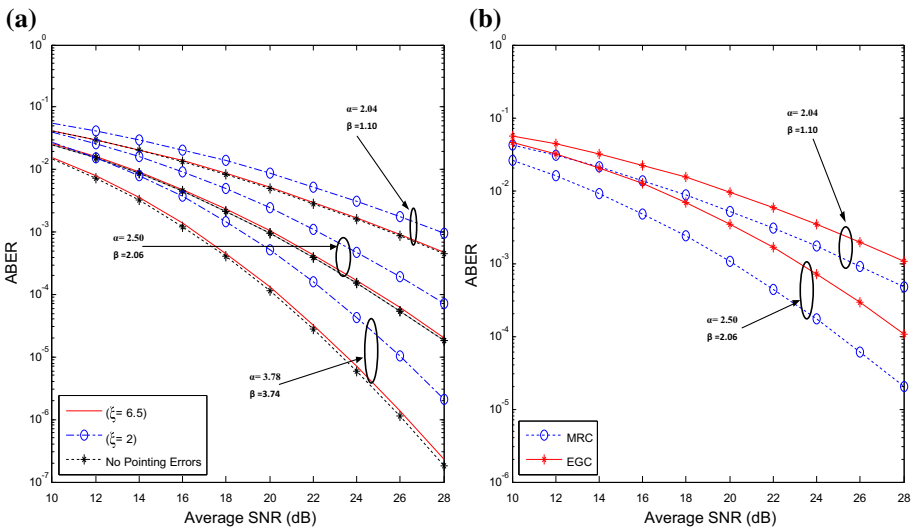


Fig. 6 a Average Error Performance of MRC SM dual-hops AF system under different values ζ and atmospheric turbulence. b Performance Comparison between MRC and EGC SM dual-hops AF system at $\zeta = 6.5$

Fig. 7 Comparison between the Capacity of MRC and EGC under various turbulence conditions without pointing error

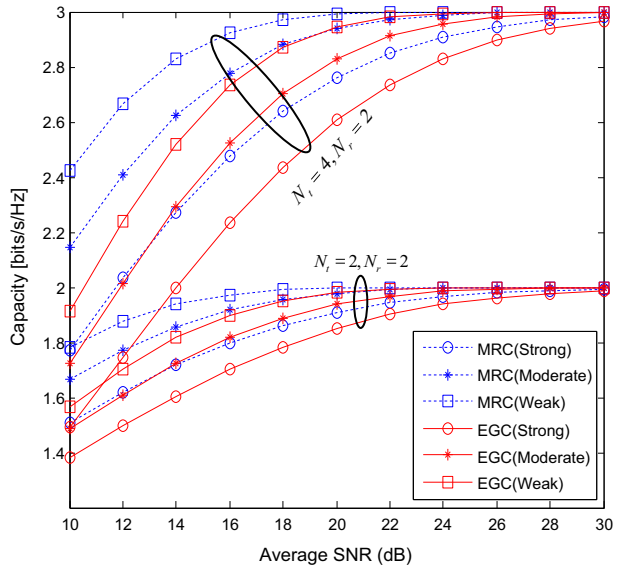
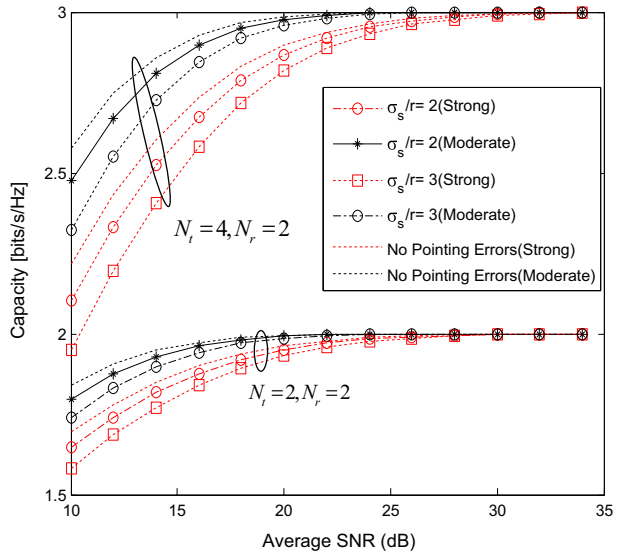


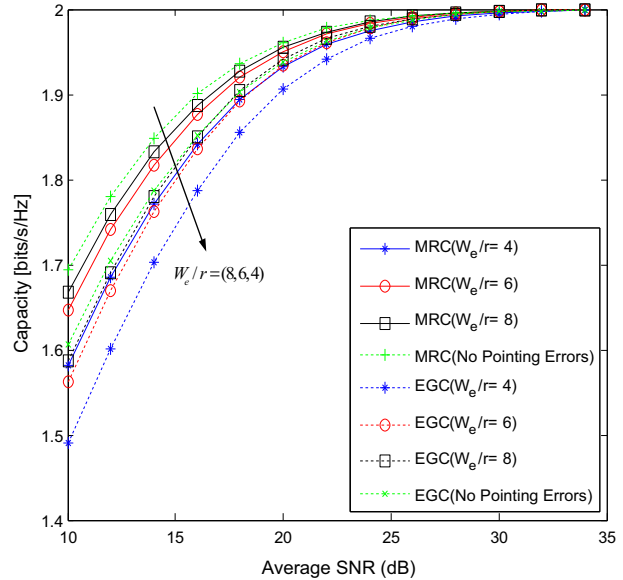
Fig. 8 Influence of pointing error on Capacity of the MRC SM dual hop AF system under different atmospheric turbulence conditions



the laser at the transmitter, the more the system capacity which is advantage of MIMO scheme specially SM with lower system complexity.

The impact of beam width on the system capacity is presented in Fig. 9. The transmitter is equipped with two lasers and the receiver makes use of MRC and EGC under a strong turbulence condition. It can be deduced that the system capacity increases with the increase in the beam width. Thus, the MRC offers the best performance. For example, at beam width of 8, the MRC system offers capacity of 1.87 bit/s/Hz compared with 1.85 bit/s/Hz at the same average SNR of 18 dB.

Fig. 9 Impact of normalized beam width on the MRC and EGC SM dual-hop AF system under strong turbulence with pointing error for $N_r^S = 2$ and $N_r^D = 2$



7 Conclusion

In this work, we analyze and evaluate the performance of optical spatial modulation heterodyne dual-hop CSI-assisted relay system with MRC and EGC combiners at the destination over Gamma–Gamma turbulence induced fading with and without pointing error. The statistical characteristics of the equivalent end-to-end SNR were derived and utilized to determine the average PEP for each combiner. The average BER close form expression for the system is then determined. The results illustrated in this paper show the significant effect of atmospheric turbulence and/or pointing error conditions on the SM-SD dual hop system. It is therefore proved that as atmospheric turbulence varies from weak to strong levels, the more the average BER and the effective system capacity degraded. Also, the result confirmed that as the pointing error increases the worst the system error and capacity become. However, large beam width at the transmitter offers the system better performance with MRC yields the best performance compared with EGC.

References

1. Kaushal, H. & Kaddoum, G. (2015). Optical communication in space: Challenges and mitigation techniques. In *IEEE communications surveys and tutorials*.
2. Andrews, L. C., Phillips, R. L., & Hopen, C. Y. (2001). *Laser beam scintillation with applications* (Vol. 99). Bellingham: SPIE Press.
3. Tsiftsis, T. A. (2008). Performance of heterodyne wireless optical communication systems over gamma-gamma atmospheric turbulence channels. *Electronics Letters*, 44(5), 373.
4. Aditi, M. & Preeti, S. (2015). Free space optics: current applications and future challenges. *International Journal of Optics*, Article ID 945483.
5. Nistazakis, H. E., Tsiftsis, T. A., & Tombras, G. S. (2009). Performance analysis of free-space optical communication systems over atmospheric turbulence channels. *IET Communications*, 3(3), 1402–1409.
6. Epple, B. (2010). Simplified channel model for simulation of free-space optical communications. *Journal of Optical Communications and Networking*, 2(5), 293–304.

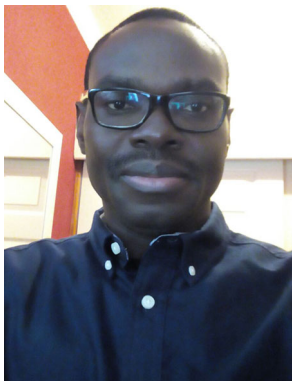
7. Popoola, W. O., Ghassemlooy, Z., & Ahmadi, V. (2008). Performance of sub-carrier modulated free-space optical communication link in negative exponential atmospheric turbulence environment. *International Journal of Autonomous and Adaptive Communications Systems*, 1(3), 342–355.
8. Al-Habash, M. A., Andrews, L. C., & Phillips, R. L. (2001). Mathematical model for the irradiance probability density function of a laser beam propagating through turbulent media. *Optical Engineering*, 40(8), 1554–1562.
9. Trung, H. D., & Pham, A. T. (2014). Pointing error effects on performance of free-space optical communication systems using SC-QAM signals over atmospheric turbulence channels. *AEU-International Journal of Electronics and Communications*, 68(9), 869–876.
10. García-Zambrana, A., Castillo-Vázquez, B., & Castillo-Vázquez, C. (2012). Asymptotic error-rate analysis of FSO links using transmit laser selection over gamma-gamma atmospheric turbulence channels with pointing errors. *Optics Express*, 20(3), 2096–2109.
11. Lee, I. E., Ghassemlooy, Z., & Ng, W. P. (2012). Effects of aperture averaging and beam width on Gaussian free space optical links in the presence of atmospheric turbulence and pointing error. In *2012 14th International conference on transparent optical networks (ICTON)* (pp. 1–4). IEEE.
12. Krishnan, P., & Kumar, D. S. (2014). Bit error rate analysis of free-space optical system with spatial diversity over strong atmospheric turbulence channel with pointing errors. *Optical Engineering*, 53(12), 126108.
13. Sandalidis, H. G., Tsiptsis, T. A., & Karagiannidis, G. K. (2009). Optical wireless communications with heterodyne detection over turbulence channels with pointing errors. *Journal of Lightwave Technology*, 27(20), 4440–4445.
14. Datsikas, C. K., Peppas, K. P., Sagias, N. C., & Tombras, G. S. (2010). Serial free-space optical relaying communications over gamma-gamma atmospheric turbulence channels. *Journal of Optical Communications and Networking*, 2(8), 576–586.
15. Acampora, A. S., & Krishnamurthy, S. V. (1999). A broadband wireless access network based on mesh-connected free-space optical links. *IEEE Personal Communications*, 6(5), 62–65.
16. Akella, J., Yuksel, M., & Kalyanaraman, S. (2005). Error analysis of multi-hop free-space optical communication. In *IEEE international conference on communications. ICC 2005* (Vol. 3, pp. 1777–1781) IEEE.
17. Tsiptsis, T. A., Sandalidis, H. G., Karagiannidis, G. K., & Sagias, N. C. (2006). Multihop free-space optical communications over strong turbulence channels. In *2006 IEEE international conference on communications* (Vol. 6, pp. 2755–2759). IEEE.
18. Anees, S., & Bhatnagar, M. R. (2015). Performance evaluation of decode-and-forward dual-hop asymmetric radio frequency-free space optical communication system. *IET Optoelectronics*, 9(5), 232–240.
19. Tang, X., Wang, Z., Xu, Z., & Ghassemlooy, Z. (2014). Multihop free-space optical communications over turbulence channels with pointing errors using heterodyne detection. *Journal of Lightwave Technology*, 32(15), 2597–2604.
20. Kazemlou, S., Hranilovic, S., & Kumar, S. (2011). All-optical multihop free-space optical communication systems. *Journal of Lightwave Technology*, 29(18), 2663–2669.
21. Peppas, K. P., Stassinakis, A. N., Nistazakis, H. E., & Tombras, G. S. (2013). Capacity analysis of dual amplify-and-forward relayed free-space optical communication systems over turbulence channels with pointing errors. *Journal of Optical Communications and Networking*, 5(9), 1032–1042.
22. Popoola, W. O., & Ghassemlooy, Z. (2009). BPSK subcarrier intensity modulated free-space optical communications in atmospheric turbulence. *Journal of Lightwave Technology*, 27(8), 967–973.
23. Aggarwal, M., Garg, P., & Puri, P. (2014). Dual-hop optical wireless relaying over turbulence channels with pointing error impairments. *Journal of Lightwave Technology*, 32(9), 1821–1828.
24. You, R., & Kahn, J. M. (2001). Average power reduction techniques for multiple-subcarrier intensity-modulated optical signals. *IEEE Transactions on Communications*, 49(12), 2164–2171.
25. Park, J., Lee, E., Chae, C. B., & Yoon, G. (2015). Outage probability analysis of a coherent FSO amplify-and-forward relaying system. *IEEE Photonics Technology Letters*, 27(11), 1204–1207.
26. Hwang, S. H., & Cheng, Y. (2014). SIM/SM-aided free-space optical communication with receiver diversity. *Journal of Lightwave Technology*, 32(14), 2443–2450.
27. Ozbilgin, T., & Koca, M. (2015). Optical spatial modulation over atmospheric turbulence channels. *Journal of Lightwave Technology*, 33, 2313–2323.
28. Peppas, K. P., & Mathiopoulou, P. T. (2015). Free space optical communication with spatial modulation and coherent detection over H-K atmospheric turbulence channels. *Journal of Lightwaves Technology*, 33(20), 4221–4232.
29. Som, P., & Chockalingam, A. (2013). BER analysis of space shift keying in cooperative multi-hop multi-branch DF relaying. In *IEEE 78th vehicular technology conference (VTC Fall)* (pp. 1–5). IEEE.

30. Som, P. & Chockalingam, A. (2013). End-to-end BER analysis of space shift keying in decode-and-forward cooperative relaying. In *2013 IEEE wireless communications and networking conference (WCNC)* (pp. 3465–3470). IEEE.
31. Yang, P., Zhang, B., Xiao, Y., Dong, B., Li, S., El-Hajjar, M., et al. (2013). Detect-and-forward relaying aided cooperative spatial modulation for wireless networks. *IEEE Transactions on Communications*, *61*(11), 4500–4511.
32. Mesleh, R., Ikki, S.S., Alwakeel, M. On the performance of dual-hop space shift keying with single amplify-and-forward relay. In *2012 IEEE wireless communications and networking conference (WCNC)* (pp. 776–780). IEEE.
33. Mesleh, R., & Ikki, S. S. (2015). Space shift keying with amplify-and-forward MIMO relaying. *Transactions on Emerging Telecommunications Technologies*, *26*(4), 520–531.
34. Mesleh, R., Elgala, H., & Haas, H. (2011). Optical spatial modulation. *IEEE Journal of Optical Communications and Networking*, *3*(3), 234–244.
35. Serafimovski, N., Younis, A., Mesleh, R., et al. (2013). Practical implementation of spatial modulation. *IEEE Transaction on Vehicular Technology*, *62*(9), 4511–4523.
36. Navidpour, S. M., Uysal, M., & Kavehrad, M. (2007). BER performance of free-space optical transmission with spatial diversity. *IEEE Transactions on Wireless Communications*, *6*(8), 2813–2819.
37. Krishnan, P., & Kumar, D. S. (2014). Performance analysis of free-space optical systems employing binary polarization shift keying signaling over gamma-gamma channel with pointing errors. *Optical Engineering*, *53*(7), 076105.
38. Bayaki, E., & Schober, R. (2012). Performance and design of coherent and differential space-time coded FSO systems. *Journal of Lightwave Technology*, *30*(11), 1569–1577.
39. Alexander, S. B. (1997). *Optical communication receiver design*. Bellingham, Washington: SPIE Optical engineering press.
40. Niu, M., Cheng, J., & Holzman, J. F. (2011). Error rate analysis of M-ary coherent free-space optical communication systems with K-distributed turbulence. *IEEE Transactions on Communications*, *59*(3), 664–668.
41. Jeganathan, J., Ghayeb, A., & Szczecinski, L. (2008). Spatial modulation: Optimal detection and performance analysis. *IEEE Communication Letters*, *12*, 1–3.
42. Karagiannidis, G. K., Tsiftsis, T. A., & Mallik, R. K. (2006). Bounds for multihop relayed communications in Nakagami-m fading. *IEEE Transactions on Communications*, *54*(1), 18–22.
43. Andrews, L. C., & Phillips, R. L. (2005). *Laser beam propagation through random media*. Bellingham, WA: SPIE.
44. Xuegui, S., & Cheng, J. (2013). Subcarrier intensity modulated MIMO optical communications in atmospheric turbulence. *Journal of Optical Communications and Networking*, *5*, 1001–1009.
45. Adamchik, V. S. & Marichev, O. I. (1990). The algorithm for calculating integrals of hypergeometric type functions and its realization in REDUCE system. In *Proceedings of the international symposium on symbolic and algebraic computation* (pp. 212–224). ACM.
46. Song, X., & Cheng, J. (2012). Alamouti-type STBC for subcarrier intensity modulated wireless optical communications. In *Global Communications Conference (GLOBECOM), 2012 IEEE* (pp. 2936–2940). IEEE.
47. Prabu, K., & Kumar, D. S. (2015). MIMO free-space optical communication employing coherent BPOLSK modulation in atmospheric optical turbulence channel with pointing errors. *Optics Communications*, *343*, 188–194.
48. Farid, A. A., & Hranilovic, S. (2007). Outage capacity optimization for free-space optical links with pointing errors. *Journal of Lightwave Technology*, *25*(7), 1702–1710.
49. Bhatnagar, M. R., & Anees, S. (2015). On the performance of Alamouti scheme in Gamma-Gamma fading FSO links with pointing errors. *IEEE Wireless Communications Letters*, *4*(1), 94–97.
50. Gradshteyn, I. S., & Ryzhik, I. M. (2014). *Table of integrals, series, and products*. London: Academic Press.
51. Prudnikov, A., Brychkov, Y., & Marichev, O. (1992). *Integrals and series, volume 4: Direct laplace transforms*. Boca Raton: CRC.
52. Skraparlis, D., Sakarellos, V. K., Panagopoulos, A. D., & Kanellopoulos, J. D. (2009). Performance of N-branch receive diversity combining in correlated lognormal channels. *IEEE Communications Letters*, *13*(7), 489–491.
53. Simon, M. K., & Alouini, M. S. (1998). A unified approach to the performance analysis of digital communication over generalized fading channels. *Proceedings of the IEEE*, *86*(9), 1860–1877.
54. Tang, X., Xu, Z., & Ghassemlooy, Z. (2013). Coherent polarization modulated transmission through MIMO atmospheric optical turbulence channel. *Journal of Lightwave Technology*, *31*(20), 3221–3228.

55. Chatzidiamentis, N. D., & Karagiannidis, G. K. (2011). On the distribution of the sum of gamma-gamma variates and applications in RF and optical wireless communications. *IEEE Transactions on Communications*, 59(5), 1298–1308.
56. Soujeri, E., & Kaddoum, G. (2015). Performance comparison of spatial modulation detectors under channel impairments. In *2015 IEEE international conference on ubiquitous wireless broadband (ICUWB)* (pp. 1–5). IEEE.
57. Anees, S., & Bhatnagar, M. R. (2015). Performance of an amplify-and-forward dual-hop asymmetric RF–FSO communication system. *Journal of Optical Communications and Networking*, 7(2), 124–135.
58. Soujeri, E., & Kaddoum, G. (2016). The impact of antenna switching time on spatial modulation. *IEEE Wireless Communications Letters*, 5(3), 256–259.
59. Prisecaru, F. A. (2010). *Mutual information and capacity of spatial modulation systems*. Bremen, Germany, Tech. Rep: Jacobs University.



Kehinde Oluwasesan Odeyemi received his B.Tech. degree in Electronic Engineering from Ladoke Akintola University of Technology Ogbomosho, Oyo State, Nigeria, in 2008. He later obtained an M.Tech. degree in the same field from the Federal University of Technology, Akure in 2012. In 2012, he joined the department of Electrical and Electronic Engineering, University of Ibadan, Nigeria where is currently working as Lecturer. He is a member of The Council for the Regulation of Engineering in Nigeria (COREN). He is currently pursuing his Ph.D. degree in Electronic Engineering at the University of KwaZulu-Natal, Durban, South Africa. He has written several research articles and his research interests are in the antenna design, optical wireless communications, diversity combining techniques and MIMO systems.



Pius Adewale Owolawi received his B.Tech. degree in Physics/Electronics from the Federal University of Technology, Akure, in 2001. He then obtained an M.Sc. and Ph.D. degrees in Electronic Engineering from the University of KwaZulu-Natal in 2006 and 2010, respectively. He holds several industry certifications such as CCNA, CCNP, CWNP, CFOA, CFOS/D and MCITP. Member of several professional bodies like SAIEE, IEEE, and SA AMSAT. In February 2007, he joined the faculty of the Engineering, Department of Electrical Engineering at Mangosuthu University of Technology, South Africa, where is currently the acting head of department. His research interests are in the computational of Electromagnetic, modelling of radio wave propagation at high frequency, fiber optic communication, radio planning and optimization techniques and renewable energy. He has written several research articles and serves as a reviewer for many scientific journals.



Prof. Viranjay M. Srivastava is a Doctorate (2012) in the field of RF Microelectronics and VLSI Design from Jaypee University of Information Technology, Solan, Himachal Pradesh, India and received the Master degree (2008) in VLSI design from Centre for Development of Advanced Computing (C-DAC), Noida, India and the Bachelor degree (2002) in Electronics and Instrumentation Engineering from the Rohilkhand University, Bareilly, India. He was with the Semiconductor Process and Wafer Fabrication Centre of BEL Laboratories, Bangalore, India, where he worked on characterization of MOS devices, fabrication of devices and development of circuit design. Currently, he is a faculty in Department of Electronics Engineering, School of Engineering, Howard College, University of KwaZulu-Natal, Durban, South Africa. His research and teaching interests includes VLSI design, Nanotechnology, RF design and CAD with particular emphasis in low-power design, Chip designing, Antenna Designing, VLSI testing and verification and Wireless communication

systems. He has more than 11 years of teaching and research experience in the area of VLSI design, RFIC design, and Analog IC design. He has supervised a number of B.Tech. and M.Tech. theses. He is a member of IEEE, ACEEE and IACSIT. He has worked as a reviewer for several conferences and Journals both national and international. He is author of more than 80 scientific contributions including articles in international refereed Journals and Conferences and also author of following books, (1) VLSI Technology, (2) Characterization of C-V curves and Analysis, Using VEE Pro Software: After Fabrication of MOS Device, and (3) MOSFET Technologies for Double-Pole Four Throw Radio Frequency Switch, Springer International Publishing, Switzerland, October 2013.